Radiation sensitivity assay with a panel of patient-derived spheroids of small cell carcinoma of the cervix

Manuscript number: Ref.: IJC-14-2869

Authors:

Aya Nakajima[1,4], Hiroko Endo[1], Hiroaki Okuyama[2], Yumiko Kiyohara[1,5], Tadashi Kimura[5], Shoji Kamiura[3], Masahiro Hiraoka[4], Masahiro Inoue[1]

Affiliations:

[1]Department of Biochemistry

[2]Department of Pathology

[3]Department of Gynecology, Osaka Medical Center for Cancer and Cardiovascular Diseases, Osaka, Japan

[4]Department of Radiation Oncology and Image-applied Therapy, Graduate School of Medicine, Kyoto University, Kyoto, Japan

[5]Department of Obstetrics and Gynecology, Osaka University Graduate School of Medicine, Suita, Japan

Conflict of Interest: The authors disclose no conflict of interest.

Short title: Radiation Sensitivity Assay with Patient-derived Culture

Corresponding author:

Masahiro Inoue

1-3-3 Nakamichi, Higashinari-ku, Osaka City, Osaka, Japan

Telephone: +81-6-6972-1181, Fax: +81-6-6973-5691

E-mail: inoue-ma2@mc.pre.osaka.jp

Keywords: small cell carcinoma of the cervix, radiation resistance, radiation-activated signaling pathways, primary culture

Abbreviations: SCCC: small cell carcinoma of the cervix; CTOS: cancer tissue–originated spheroid; HIF-1: hypoxia-inducible factor-1; HSP90: heat shock protein 90; ROS: reactive oxygen species; mTOR: mammalian target of rapamycin; shRNA: short hairpin RNA

Article category: Cancer Therapy

The novelty and impact of the work:

Small cell carcinoma of the uterine cervix (SCCC) is a rare and aggressive disease lacking research platforms. Here we have established 6 lines of patient-derived spheroid cultures of SCCC by our recently developed culture methods. We demonstrate that a panel of patient-derived cultures representing the diversity of the disease and its application to assays predicting response to therapies contribute to basic biology as well as to developing treatment strategies, especially for rare cancers like SCCC.

Abstract

Small cell carcinoma of the uterine cervix (SCCC) is a rare cancer with a poor prognosis for which no standard treatment exists. Here we successfully established panels of patient-derived spheroid cultures from six SCCC patient samples by cancer tissue–originated spheroids (CTOS) method. To assess the intrinsic radio-sensitivity and mechanism of radio-resistance in individual SCCC patients, we further developed an *in vitro* sensitivity assay for radiation. Radiation sensitivity in the CTOS assay varied among individual cases and was consistent with *in vivo* radiation sensitivity using CTOS-derived xenograft tumors in the examined cases. Furthermore, by comparing gene expression in CTOSs with different radio-sensitivity, we found that expression of hypoxia-inducible factor-1α (HIF-1α) target genes was up-regulated in resistant CTOSs. HIF-1α protein levels increased several hours after irradiation. In a radio-resistant CTOS, an inhibitor of heat shock protein 90 (HSP90) suppressed radiation-induced HIF-1α expression. Suppression of HIF-1α by small hairpin RNA significantly enhanced the effect of radiation, at least in part by promoting radiation-induced apoptosis. HSP90 inhibitor also increased radiation sensitivity. Our results indicate that radiation-induced HIF-1α up-regulation was one mechanism of radio-resistance in a radio-resistant SCCC CTOS. Accumulating CTOS lines may provide a good platform to study characters of rare cancers like SCCC.

Introduction

Small cell carcinoma of the uterine cervix (SCCC) is a neuroendocrine cancer and rare, accounting for up to 2% of all cervical carcinomas, although the incidence is increasing as a result of improved recognition and diagnostic accuracy [1, 2]. SCCC is a highly aggressive disease, and because of early onset of metastasis, has a much worse prognosis compared with stage-comparable poorly differentiated squamous cell carcinoma of the cervix [3-5]. Multimodality treatments including surgical resection, radiation therapy, and chemotherapy for small cell carcinoma of the lung have been applied to SCCC because of their pathological similarity; however, a clear treatment algorithm remains difficult to develop for SCCC because of its rarity [1, 2].

Radiation therapy is one of the current modalities for SCCC [2, 5, 6]. It is widely accepted that the sensitivity of cancer to radiation therapy is quite diverse in individual patients. In cervical cancer, much effort has targeted developing biomarkers for predicting radiation sensitivity including analysis of protein expression by immunohistochemistry [7] and gene expression by DNA microarray analysis [8, 9] and HPV subtypes [10, 11]. Other non-molecular biomarkers such as evaluating intra-tumoral hypoxia measured by oxygen electrode [12] and fluorodeoxyglucose-positron emission tomography [13] have also been investigated in cervical cancer patients. Although some of these biomarkers correlate with response to radiotherapy or prognosis [7-13], no predictive assay is currently available in routine clinical radiation oncology.

An alternative approach to predicting radiation sensitivity of patient tumors is measuring the

intrinsic radio-sensitivity of cancer cells cultured *ex vivo*. In cervical cancer, an *in vitro* culture–based sensitivity assay using a clonogenic assay or ^{3}H-thymidine incorporation is reported to correlate with outcome in patients treated with radiotherapy [14, 15]. However, technical issues including a laborious, time-consuming, and poorly reproducible procedure have hampered clinical application. Recently, we developed a novel method for primary culture of human cancer cells from colorectal, urothelial, and lung cancer, which we have designated as the cancer tissue–originated spheroid (CTOS) method [16-18]. In the CTOS method, cell–cell contact is maintained throughout preparation and culture of the cancer cells. With this approach, cancer cells with high purity and high efficiency can be feasibly isolated from patient samples. CTOSs and CTOS-derived xenografts preserve characteristics of original tumors such as gene mutation status and cell differentiation [16].

In this study, we applied the CTOS method to human SCCC and developed a novel *in vitro* radiation sensitivity assay. We then investigated the mechanism of radiation resistance by comparing CTOSs with different radio-sensitivity.

Materials and Methods

CTOS preparation, culture, and storage

This study was approved by the institutional ethics committees at Osaka Medical Center for Cancer and Cardiovascular Diseases and Osaka University. Surgical specimens were obtained from patients treated with radical hysterectomy at either hospital upon informed consent. Preparation and culture

of CTOSs were performed according to a previously described protocol [16]. Briefly, surgical samples or xenograft tumors of non-obese diabetic/severe combined immunodeficiency (NOD/SCID) mice were digested with liberase DH (Roche Applied Science, Mannheim, Germany) and filtered through cell strainers. Fragments on the 100-μm or 40-μm cell strainer (BD Falcon, Franklin Lakes, NJ) were collected. For culture, CTOSs were embedded in BD Matrigel Matrix Growth Factor Reduced (GFR) (BD Biosciences, San Jose, CA) and cultured in StemPro hESC (Invitrogen, Carlsbad, CA). For CTOS storage, CTOSs were mildly digested with 0.25% trypsin-EDTA (Life Technologies, Carlsbad, CA), suspended with CELLBANKER 1 (Nippon Zenyaku Kogyo, Fukushima, Japan) containing 10 μM Y-27632 (Wako Pure Chemical Industries, Osaka, Japan), and frozen at -80ºC.

Immunohistochemistry

Immunohistochemistry was performed as previously described [16]. The primary antibodies against CD56 (Clone 1B6) were obtained from MBL (Nagoya, Japan); synaptophysin (Clone SY38) from Dako (Glostrup, Denmark); chromogranin A from Abcam (Cambridge, UK); HIF-1α (clone 54) from BD Transduction Laboratories (San Jose, CA); and phospho-histone H2A.X (γH2AX) (Ser139) from Cell Signaling Technologies (Danvers, MA). For scoring γH2AX expression, the number of nuclei with one or more foci and total number of nuclei were counted in 8–10 CTOSs in each group. For pimonidazole staining, CTOSs were incubated with 200 μM Hypoxyprobe^{TM}-1 (HPI, Burlington, MA) for 2 hours before fixation, then immunostained following the manufacturer's instructions. For

whole mount immunostaining, CTOSs were fixed and permeabilized with 4% paraformaldehyde/PBS containing 1% TritonX-100 at 4ºC for an hour. After being blocked with 5% goat serum/PBS-T for an hour, CTOSs were incubated with anti-HIF-1α antibody overnight, then with Alexa-555–conjugated secondary antibody (Moleculer Probes, Eugene, OR) overnight. After counterstaining with Hoechst33342 (Molecular Probes), CTOSs were mounted with FluorSave Reagent (Calbiochem, San Diego, CA). Fluorescence images were obtained using confocal microscopy (TCS SPE, Leica Microsystems, Wetzlar, Germany).

Western blot

CTOSs were lysed with cell lysis buffer (10 mM Tris (pH 7.4), 0.15 M NaCl, 1% NP40, 0.25% sodium deoxycholate, 0.05 M NaF, 2 mM EDTA, 0.1% SDS, 2 mM $NaVO_4$, 10 μg/mL aprotinin, 10 μg/mL leupeptin, and 1 mM PMSF). Western blot was performed as previously described [18]. Primary antibodies used against phospho-S6 (Ser235/236), caspase-3, and cleaved caspase-3 (Asp175) were obtained from Cell Signaling Technologies; HIF-1α (clone 54) from BD Transduction Laboratories; HIF-2α from Novus Biologicals (Littleton, CO); and β-actin from Sigma-Aldrich (Saint Louis, MO).

Reagents

RAD001 was purchased from Toronto Research Chemicals (Toronto, Ontario, Canada) and 17-AAG from Cell Signaling Technologies. These reagents were dissolved in dimethyl sulfoxide (DMSO)

(Sigma-Aldrich), to a concentration of 1 mM stock solution.

Radio-sensitivity assay

For the radiation sensitivity assay, each CTOS was embedded in a gel droplet of Matrigel GFR and pre-incubated in StemPro hESC for 24 hours before being irradiated at the indicated dose using the MBR-1505R irradiator (Hitachi, Tokyo, Japan) at a dose rate of 0.25 Gy/min. CTOS viability was evaluated based on CTOS size at day 7, corrected by the CTOS size at day 0. Images were taken at ×10 magnification using an OLYMPUS IX70 microscope (OLYMPUS, Tokyo, Japan). CTOS size was measured using image analysis software (Image J; National Institutes of Health, Bethesda, MD). For staining of dead cells at day 7, propidium iodide (Calbiochem) was added to the medium at a concentration of 1 μg/mL and incubated at 37ºC for 10 min. After CTOSs were washed, fluorescence images were obtained.

For 17-AAG treatment, CTOSs were embedded in Matrigel GFR and cultured in StemPro hESC containing 17-AAG (1 μM). CTOSs were exposed to the drug for an initial 72 hours, then washed and incubated without drug afterwards. Control CTOSs were treated in parallel with respective concentrations of DMSO as a vehicle control. CTOS viability was evaluated by size as described above.

Measurement of reactive oxygen species (ROS) levels

CTOSs were labeled with 10 μM dichlorofluorescin diacetate (DCFDA) for 50 minutes, washed with culture medium, and analyzed using fluorescence microscopy. CTOSs treated with N-acetylcysteine (20 mM, Senjyu Pharmaceutical Co., Osaka, Japan) were used as negative control.

Gene expression analysis

Total RNA was extracted from CTOSs embedded in Matrigel for 24 hours, using TRIzol Reagent (Life Technologies), and purified by RNeasy Mini Kit (QIAGEN, Germantown, MA). Microarray hybridizations were performed at Hokkaido System Science Co. Ltd. (Sapporo, Japan) using SurePrint G3 Human GE 8x60K (Agilent Technologies, Santa Clara, CA). The microarray slides were scanned and gene expression profiles analyzed at Hokkaido System Science according to the manufacturer's protocol. Microarray data have been submitted to GEO (Series GSE56540). Gene set enrichment analysis was performed using default settings [19]. The list of HIF-1α target genes [20] was obtained from the Molecular Signature Database. For semi-quantitative RT-PCR, one microgram of total RNA was reverse transcribed to obtain cDNA using Superscript III (Invitrogen) according to the manufacturer's protocol. The PCR reactions were done with the Gene Amp® PCR System (Life Technologies). The primer sequences are shown in Supplementary Table 1.

Plasmid construction and gene transfer to CTOS

pPiggyBac (PB)-Ubc.eGFP-neo and pCMV-hyPBase were gifts from Dr. Yusa, Wellcome Trust

Sanger Institute, Cambridge, UK [21]. For making short hairpin (sh) RNA vectors targeting HIF-1α, the EcoRI–XhoI fragments including the H1 promoter and shRNA target sequences from pSuperRetro/shRNA/HIF-1α plasmids (Endo et al., PlosOne, in press) were transferred to pPB-Ubc.eGFP-neo to make pPB shRNA/HIF-1α#1 and #3. The target sequences were 5'-GATGACATGAAAGCACAGA-3' for pPBneo/shHIF-1α#1 and 5'-GACAGTACAGGATGCTTGC-3' for pPBneo/HIF-1α#3, respectively. For electroporation, CTOSs were pretreated with 5 mM EDTA/PBS for 30 minutes at room temperature, then mixed with vectors of shRNA and the transposase expression vector pCMV-hyPBase. Electroporation was performed in 2-mm gap cuvettes at 150 V for 5 ms using a Type II NEPA21 electroporator (Nepa Gene, Chiba, Japan). After transfection, CTOSs were selected with G-418 (Roche Applied Science) and maintained in medium containing G-418. CTOSs transfected with pPB-Ubc.eGFP-neo were used as a transfection control.

Animal studies

Animal studies were performed in compliance with the guidelines of the institutional animal study committee of Osaka Medical Center for Cancer and Cardiovascular Diseases. For CTOS passages, small pieces of a tumor specimen or CTOS/Matrigel mixture were implanted subcutaneously into the flank of 4-week-old female NOD/SCID mice (CLEA Japan, Shizuoka, Japan). For the *in vivo* radiation experiment, the xenografts were generated by implanting CTOSs with Matrigel into cohorts

of 4-week-old female BALB/cAJcl-*nu/nu* mice (CLEA Japan). The mice were X-ray irradiated with 5 Gy when tumor volume reached 120–160 mm^3, using a MBR-1505R irradiator at a dose rate of 0.1 Gy/min. Tumor volume was measured every 2 or 3 days and calculated with the formula $0.5XT_{width}{}^2XT_{length}$.

Statistical analysis

Statistical analysis was carried out with GraphPad Prism 6 (GraphPad Software, San Diego, CA). The statistical significance was tested using unpaired *t*-tests. Values of $p < 0.05$ were considered to indicate statistical significance.

Results

CTOSs were prepared from six SCCCs according to the protocol described in a previous report [16] (Supplementary Table 2). Although the flow-through fraction mostly consisted of single cells with few small aggregates (Fig. 1*a*, left), the organoid fraction consisted of irregular cell masses in all six cases (Fig. 1*a*, middle), which turned into round spheroids with smooth edges after 2 days of culture in suspension, as previously described in other cancers [16-18] (Fig. 1*a*, right). All six CTOSs formed tumors in the subcutaneous region of NOD-SCID mice. The histological features of the xenograft tumors, including small cell size, high N/C ratio and nuclear molding, were similar to that of the original patient tumors (Fig. 1*b*). Cancer cells of the CTOSs were also morphologically similar to

those of the original tumors, and CTOSs consisted of pure cancer cells, as has been previously reported [16-18]. Neuroendocrine differentiation, which is often observed in SCCC, was also retained in CTOSs and CTOS-derived xenografts (Fig. 1*c*). The expression of neuroendocrine markers in original tumors and CTOSs was further evaluated by quantitative RT-PCR in all cases (Supplementary fig. 1). The expression pattern of neuroendocrine markers was mostly retained in CTOSs with minor exceptions. For further studies, we used CTOSs prepared from xenograft tumors in early passages (fewer than six passages).

Because radiation therapy is a current modality for small cell carcinoma [2, 5, 6], we tested the radiation sensitivity in all six SCCC CTOSs. Irradiated CTOSs showed morphological characteristics of an irregular surface and decreased transparency and brightness (Fig. 2*a*). This morphological change was associated with cell death detected by propidium iodide staining. We assessed CTOS radio-sensitivity by evaluating growth inhibition at 1 week after irradiation. CTOS growth was suppressed by radiation in a dose-dependent manner, and each CTOS showed a substantial difference in radiation sensitivity (Fig. 2*b*). The growth rate, which also had substantial difference among CTOSs, was not correlated with radiation sensitivity (Fig. 2*c*). In addition, radiation sensitivity of xenograft-derived CTOSs was compatible with that of corresponding patient-derived CTOSs (Supplementary fig. 2).

Next, we investigated the radiation effects *in vivo* (Fig. 3*a*). Tumors derived from cerv-5 and cerv-21, which was resistant *in vitro*, did not show apparent regression and regrew with delay. In

contrast, tumors from cerv-9, which were sensitive *in vitro*, showed clear regression after radiation. Taken together, the *in vitro* radiation sensitivity assay results using different SCCC CTOSs were consistent with *in vivo* experiments.

We also performed a γH2AX foci formation assay, which has been reported to be associated with intrinsic radio-sensitivity [22]. Radio-resistant cerv-5 and cerv-21 showed enhanced DNA repair ability as evidenced by the reduced number of residual γH2AX foci 24 hours after irradiation compared to radio-sensitive cerv-9 and cerv-46 (Fig. 3*b*, *c*). We further observed profound radiation-induced apoptosis in radio-sensitive CTOSs (Fig. 3*e*).

Next, we focused on cerv-5, which was one of the most radio-resistant CTOSs, and investigated the mechanism of radio-resistance in this particular case. First, we employed microarray analysis of gene expression to find factors that affect radio-sensitivity by comparing cerv-5 and a radio-sensitive CTOS (cerv-9). Gene set enrichment analysis revealed that HIF-1α target genes are highly up-regulated at basal levels in cerv-5 compared with cerv-9 (Fig. 4*a*). Some of the HIF-1α target genes were validated by RT-PCR in CTOSs. Radio-sensitive cerv-9 showed exceptionally low levels of expression of HIF-1α target genes (Fig. 4*b*). The expression of HIF-1α and its target genes was further evaluated by quantitative RT-PCR in all CTOSs (Supplementary fig.3*a*), revealing that cerv-5 had relatively high levels of HIF-1α and its target genes among the cases. HIF-1α protein was undetectable at basal levels in CTOSs. However, HIF-1α protein was highly induced at 4 hours after radiation in cerv-5, poorly in cerv-9, and moderately in other CTOSs (Fig. 4*c*). Radiation-induced

HIF-1α in cerv-5 was confirmed by immunostaining (Fig. 4*d*). The basal levels of HIF-2α varied among patients. Especially, HIF-2α was not expressed in cerv-5, which showed highest levels of HIF-1α downstream genes (Supplementary fig. 3*b*). We further investigated the mechanism that mediated radiation-induced up-regulation of HIF-1α using cerv-5 CTOSs. First, we examined whether hypoxia was responsible for HIF-1α induction. The pimonidazole-positive area was not increased after irradiation while it was detected in the center of large CTOSs and in all cells in CTOSs under 1% oxygen conditions (Fig. 5*a*). This outcome suggests that the HIF-1α induction by radiation was not likely due to hypoxia.

HIF-1α activity is reportedly increased after radiation by various mechanisms including production of ROS, activation of the Akt/mammalian target of rapamycin (mTOR) pathway, and stabilization by heat shock protein 90 (HSP90) [23-26]. To determine the involvement of ROS, we assessed ROS levels using the ROS-sensitive dye DCFDA (Fig. 5*b*). Basal levels of DCFDA fluorescence were detected in CTOSs, which were reduced by N-acetylcysteine. However, the DCFDA fluorescence levels did not increase after radiation, indicating that HIF-1α up-regulation was not the result of increased ROS production.

In cerv-5, the levels of phospho-S6 were comparable in control and irradiated CTOSs, indicating that basal levels of mTOR activity were high under the culture conditions but did not change after irradiation (Fig. 5*c*). In addition, although treatment with RAD001, an mTOR inhibitor, suppressed mTOR activity even at low concentrations, RAD001 had no effect on the levels of

HIF-1α after radiation, indicating that radiation-induced HIF-1α expression was not the result of activation of the mTOR pathway. Last, we examined whether HSP90 contributed to radiation-induced HIF-1α up-regulation (Fig. 5*d*). Treatment with 17-AAG, an HSP90 inhibitor, effectively inhibited HIF-1α induction, suggesting that radiation-induced HIF-1α was at least partly the result of protein stabilization by HSP90.

We further investigated the role of HIF-1α in radiation resistance in cerv-5. The levels of HIF-1α were forcibly suppressed by shRNA, which was confirmed by immunostaining (Fig. 6*a*). The efficacy of HIF-1α knockdown was also confirmed by decreased expression of HIF-1α target genes (Supplementary fig. 4*a*). The radio-sensitivity of the cerv-5 CTOS was significantly increased when HIF-1α levels were suppressed by shRNA (Fig. 6*b*, left and middle). We also tested whether the pharmacological inhibition of HIF-1α increases radio-sensitivity. Effect of 17-AAG alone was varied among CTOSs (Supplementary fig. 4*b*). Although cerv-5 CTOSs required relatively high dose of 17-AAG to be effective (around 1 μM), the combined treatment of 17-AAG and radiation suppressed the growth of CTOSs significantly more than did radiation alone (Fig. 6*b*, right). Cerv-39, which showed relatively high levels of basal as well as radiation-induced HIF-1α, also showed synergistic effect of radiation and 17-AAG (Supplementary fig.4*c*).

Finally, we investigated the mechanism of radio-sensitization in HIF-1α knockdown CTOSs. Cleavage of caspase-3 after radiation was promoted in the HIF-1α knockdown CTOSs compared to the control CTOSs (Fig. 6*c*), although the levels were low as the cleaved form of caspase-3 was

undetectable with total caspase-3 antibody. Taken together, these results suggest that HIF-1α knockdown enhanced radiation sensitivity, at least in part because of apoptosis.

Discussion

SCCC is a rare cancer with a poor prognosis and biological features that are not well elucidated. As a research platform, even conventional cell lines are quite rare [27, 28]. We demonstrated here that CTOS lines of SCCC were easily and efficiently established from surgical samples and used them as an example, applying radiation therapy technology. The success rates of CTOS preparation and culture are 98.7% in colorectal cancer [16], 80.0% in lung cancer [18], and 84.2% in bladder cancer [17]. Some of the other cancers, including head and neck, liver, breast, pancreas, and prostate have much less success rate. In terms of the CTOS growth in culture, the success rates are much less; 79.0% in colorectal cancer and 67.2% in lung cancer. As we show in this study, success rate of CTOS preparation and culture in SCCC was both 100% (6/6 cases), which has the highest success rate among the cancer types we have examined. Although the number is still small, SCCC would be one of the most suitable caners for establishing CTOS panel. Although we reported that CTOS could be prepared from small biopsy samples in colorectal cancer [16], preparation of SCCC CTOSs from biopsy samples needs further study to be established. Accumulating a number of CTOSs could produce a platform for evaluating drug or radiation efficiency, which would be useful for basic cancer research as well as developing a therapeutic strategy, especially for rare cancers like SCCC.

Once CTOS-derived or patient-derived xenografts are established, we demonstrated in this study that CTOS method can permit feasible manipulation of cancer cells ex vivo [29].

For predicting radiation sensitivity in individual patients, several assays have been developed using biopsy samples. Although surrogate markers such as DNA break induction and repair, chromosome aberrations and apoptosis were explored, few studies have shown the correlation with the clinical outcome, partly because of insufficient reproducibility [30]. Another problem was inconsistent correlations with direct assays of radiation sensitivity in cultured cell lines [8, 31]. Recently, genome-wide analyses using patient samples have been applied to the quest for biomarkers. A combination of gene expression analysis and functional imaging is reportedly useful for predicting radio-sensitivity, although it requires further investigation for clinical application [30, 32]. On the other hand, some attempts at a sensitivity bioassay using primary culture have been reported in malignant glioma, head and neck cancer, and cervical cancer [14, 33, 34]. An advantage of this assay is that one can directly assess the response to radiation in cancer cells. However, clinical application of these 2D culture–based approaches has been limited because of the long duration (2–3 weeks for the clonogenic assay) required, low plating efficiencies, and contamination of non-tumor cells.

Growing evidence indicates that three-dimensional spheroid cultures of cancer cells are more representative of tumors *in vivo* than are monolayer cultures because cell–cell contact, interaction with the extracellular matrix, and diffusion of oxygen and nutrients may influence cancer cell behavior [35, 36]. Here we demonstrate a novel radiation sensitivity assay using CTOSs from

patient-derived xenografts. Because the preparation and culture of CTOSs directly from patient samples were equally feasible, the assay can be performed with patient biopsy samples. With this technique, several limitations of previously reported assays using primary cultured cells can be overcome including laboriousness, contamination with non-tumor cells, and poor reproducibility. In addition, we can evaluate radiation sensitivity within a week using the CTOS growth delay assay *in vitro*. With this model, we observed differential radio-sensitivity among CTOSs from individual patients. We also showed that *in vitro* radio-sensitivity in the CTOS assay parallels *in* vivo radio-sensitivity in some CTOS-derived xenotumors examined. A further advantage of the CTOS assay is that we can analyze the molecular response following irradiation. In this study, for the first time, we enabled introduction of an expression vector into CTOSs using electroporation with a PiggyBac transposon system. We found radiation-induced HIF-1α expression in SCCC CTOSs and showed that HIF-1α was associated with radiation resistance in one case. Because the CTOSs consist of pure cancer cells with no contamination of host cells, the CTOS assay might be evaluating only intrinsic sensitivity of cancer cells, excluding the effect of the tumor microenvironment. Correlation between CTOS radio-sensitivity and patient outcome remains to be determined.

HIF-1 is a transcription factor, a heterodimer composed of an O_2-regulated HIF-1α and constitutively expressed HIF-1β subunit. Under normoxia, HIF-1α protein is rapidly degraded. On the other hand, under hypoxia, HIF-1α is stabilized and interacts with HIF-1β. HIF-α is also regulated at the transcriptional and translational levels by various stimuli other than hypoxia. HIF-1

induces the expression of various genes responsible for cell survival, metabolism, angiogenesis, and invasion and metastasis in cancer cells [37]. Immunohistochemical analyses of patient tumors have shown that HIF-1α overexpression is associated with patient mortality in various cancers, including brain, breast, ovarian, and endometrial cancers [37]. In cervical cancer, HIF-1α expression is reported to be a poor prognostic factor in patients treated with radiation therapy [38].

In this study, HIF-1α target genes were up-regulated under normoxia in a subset of SCCC CTOS. HIF-1α protein was not detectable at basal levels, suggesting that basal levels of HIF-1α are sufficient to confer increased target gene expression, as reported previously [39, 40]. Moreover, we observed increased HIF-1α expression in five of six SCCC CTOSs in vitro at 4 hours after irradiation. It is rarely reported that HIF-1α levels increase after radiation in cell lines cultured in 2D conditions, with few exceptions [25, 26]. In contrast, it has been reported that intratumoral HIF-1 activity increases around 12–24 hours after radiation only *in vivo* [23, 24] but not in the cognate cell lines in standard culture conditions *in vitro*. CTOS might mimic the *in vivo* situation more than the 2D cultured cell lines do. In terms of the mechanism of up-regulation of HIF-1α after radiation, previous reports state that it is mediated by ROS generated during radiation-induced tumor reoxygenation and by activation of the Akt/mTOR signaling pathway [23, 24]. In contrast, our study suggests that it was not likely due to hypoxia, ROS, or the mTOR pathway but rather the result of stabilization through HSP90. Mechanisms of HIF-1α up-regulation after radiation might depend on cell type or culture conditions.

Although HIF-1α is reported to be a prognostic marker after radiotherapy, the impact of HIF-1 inhibition on radio-sensitivity of cancer cells is not fully understood because of the complex role of HIF-1 in tumors. HIF-1 promotes radio-resistance of the tumor vasculature through induction of vascular endothelial growth factor [41]. In our study, however, the impact of HIF-1α inhibition should be intrinsic to cancer cells because CTOS consists of pure cancer cells. We found that knockdown of HIF-1α enhanced the effect of radiation by increasing apoptosis (Fig. 6). This finding is consistent with previous reports that HIF-1 protects cells from apoptosis [42, 43]. On the other hand, HIF-1 radio-sensitizes tumors by increasing apoptotic potential, proliferation rates, and ATP metabolism [44]. Thus, it is likely that the impact of HIF-1α on radio-sensitivity is cell-type dependent.

Our data indicate that pharmacological inhibition of HIF-1α might be effective for sensitizing tumors to radiation therapy in clinical situations in some resistant cases. HSP90 and a receptor of activated protein kinase C compete for binding to HIF-1α and regulate HIF-1α protein stability [45]. We showed here that an HSP90 inhibitor sensitizes radio-resistant CTOSs along with effective blockade of radiation-induced HIF-1α expression. Several preclinical studies have already reported that HSP90 inhibitors have radio-sensitizing effects [46-48]. Although HSP90 inhibitors affect multiple proteins associated with tumor radio-sensitivity, our data indicate that HIF-1α might be a target molecule of HSP90 after radiation.

Acknowledgments

We thank A. Mizukoshi and T. Yasuda for technical assistance, and M. Izutsu for secretarial assistance. This work was supported in part by KAKENHI (22791240, 25461937) (H.E., M.I.), the Japan Advanced Molecular Imaging Program (J-AMP) of the Ministry of Education, Culture, Sports, Science, and Technology of Japan (M.I.),.the Japan Foundation for Applied Enzymology (H.E., H.O., M.I.), Takeda Science Foundation (M.I.), and The Naito Foundation (M. I.). The authors have no conflicts of interest.

References

1. Crowder S, Tuller E. Small cell carcinoma of the female genital tract. *Seminars in oncology* 2007;**34**: 57-63.

2. Gardner GJ, Reidy-Lagunes D, Gehrig PA. Neuroendocrine tumors of the gynecologic tract: A Society of Gynecologic Oncology (SGO) clinical document. *Gynecol Oncol* 2011;**122**: 190-8.

3. McCusker ME, Coté TR, Clegg LX, Tavassoli FJ. Endocrine tumors of the uterine cervix: incidence, demographics, and survival with comparison to squamous cell carcinoma. *Gynecologic Oncology* 2003;**88**: 333-9.

4. Chan JK, Loizzi V, Burger RA, Rutgers J, Monk BJ. Prognostic factors in neuroendocrine small cell cervical carcinoma: a multivariate analysis. *Cancer* 2003;**97**: 568-74.

5. Cohen JG, Kapp DS, Shin JY, Urban R, Sherman AE, Chen LM, Osann K, Chan JK. Small cell carcinoma of the cervix: treatment and survival outcomes of 188 patients. *American journal of obstetrics and gynecology* 2010;**203**: 347 e1-6.

6. Zivanovic O, Leitao MM, Jr., Park KJ, Zhao H, Diaz JP, Konner J, Alektiar K, Chi DS, Abu-Rustum NR, Aghajanian C. Small cell neuroendocrine carcinoma of the cervix: Analysis of outcome, recurrence pattern and the impact of platinum-based combination chemotherapy. *Gynecol Oncol* 2009;**112**: 590-3.

7. Noordhuis MG, Eijsink JJ, Ten Hoor KA, Roossink F, Hollema H, Arts HJ, Pras E, Maduro JH, Reyners AK, de Bock GH, Wisman GB, Schuuring E, et al. Expression of epidermal growth factor receptor

(EGFR) and activated EGFR predict poor response to (chemo)radiation and survival in cervical cancer. *Clinical cancer research : an official journal of the American Association for Cancer Research* 2009;**15**: 7389-97.

8. Klopp AH, Eifel PJ. Biological predictors of cervical cancer response to radiation therapy. *Seminars in radiation oncology* 2012;**22**: 143-50.

9. Harima Y, Togashi A, Horikoshi K, Imamura M, Sougawa M, Sawada S, Tsunoda T, Nakamura Y, Katagiri T. Prediction of outcome of advanced cervical cancer to thermoradiotherapy according to expression profiles of 35 genes selected by cDNA microarray analysis. *International journal of radiation oncology, biology, physics* 2004;**60**: 237-48.

10. Kim JY, Park S, Nam BH, Roh JW, Lee CH, Kim YH, Shin HJ, Lee SK, Kong SY, Seong MW, Han TJ, Lee MY, et al. Low initial human papilloma viral load implicates worse prognosis in patients with uterine cervical cancer treated with radiotherapy. *Journal of clinical oncology : official journal of the American Society of Clinical Oncology* 2009;**27**: 5088-93.

11. Wang CC, Lai CH, Huang HJ, Chao A, Chang CJ, Chang TC, Chou HH, Hong JH. Clinical effect of human papillomavirus genotypes in patients with cervical cancer undergoing primary radiotherapy. *International journal of radiation oncology, biology, physics* 2010;**78**: 1111-20.

12. Fyles AW, Milosevic M, Wong R, Kavanagh MC, Pintilie M, Sun A, Chapman W, Levin W, Manchul L, Keane TJ, Hill RP. Oxygenation predicts radiation response and survival in patients with cervix cancer. *Radiotherapy and oncology : journal of the European Society for Therapeutic Radiology and Oncology* 1998;**48**: 149-56.

13. Xue F, Lin LL, Dehdashti F, Miller TR, Siegel BA, Grigsby PW. F-18 fluorodeoxyglucose uptake in primary cervical cancer as an indicator of prognosis after radiation therapy. *Gynecol Oncol* 2006;**101**: 147-51.

14. West CM, Davidson SE, Roberts SA, Hunter RD. The independence of intrinsic radiosensitivity as a prognostic factor for patient response to radiotherapy of carcinoma of the cervix. *British journal of cancer* 1997;**76**: 1184-90.

15. Randall LM, Monk BJ, Moon J, Parker R, Al-Ghazi M, Wilczynski S, Fruehauf JP, Markman M, Burger RA. Prospective evaluation of an in vitro radiation resistance assay in locally advanced cancer of the uterine cervix: a Southwest Oncology Group Study. *Gynecol Oncol* 2010;**119**: 417-21.

16. Kondo J, Endo H, Okuyama H, Ishikawa O, Iishi H, Tsujii M, Ohue M, Inoue M. Retaining cell-cell contact enables preparation and culture of spheroids composed of pure primary cancer cells from colorectal cancer. *Proceedings of the National Academy of Sciences of the United States of America* 2011;**108**: 6235-40.

17. Okuyama H, Yoshida T, Endo H, Nakayama M, Nonomura N, Nishimura K, Inoue M. Involvement of heregulin/HER3 in the primary culture of human urothelial cancer. *The Journal of urology* 2013;**190**: 302-10.

18. Endo H, Okami J, Okuyama H, Kumagai T, Uchida J, Kondo J, Takehara T, Nishizawa Y, Imamura F, Higashiyama M, Inoue M. Spheroid culture of primary lung cancer cells with neuregulin

1/HER3 pathway activation. *J Thorac Oncol* 2013;**8**: 131-9.

19. Subramanian A, Tamayo P, Mootha VK, Mukherjee S, Ebert BL, Gillette MA, Paulovich A, Pomeroy SL, Golub TR, Lander ES, Mesirov JP. Gene set enrichment analysis: a knowledge-based approach for interpreting genome-wide expression profiles. *Proceedings of the National Academy of Sciences of the United States of America* 2005;**102**: 15545-50.

20. Elvidge GP, Glenny L, Appelhoff RJ, Ratcliffe PJ, Ragoussis J, Gleadle JM. Concordant regulation of gene expression by hypoxia and 2-oxoglutarate-dependent dioxygenase inhibition: the role of HIF-1alpha, HIF-2alpha, and other pathways. *The Journal of biological chemistry* 2006;**281**: 15215-26.

21. Yusa K, Zhou L, Li MA, Bradley A, Craig NL. A hyperactive piggyBac transposase for mammalian applications. *Proceedings of the National Academy of Sciences of the United States of America* 2011;**108**: 1531-6.

22. Olive PL. Retention of gammaH2AX foci as an indication of lethal DNA damage. *Radiotherapy and oncology : journal of the European Society for Therapeutic Radiology and Oncology* 2011;**101**: 18-23.

23. Moeller BJ, Cao Y, Li CY, Dewhirst MW. Radiation activates HIF-1 to regulate vascular radiosensitivity in tumors: role of reoxygenation, free radicals, and stress granules. *Cancer cell* 2004;**5**: 429-41.

24. Harada H, Itasaka S, Kizaka-Kondoh S, Shibuya K, Morinibu A, Shinomiya K, Hiraoka M. The Akt/mTOR pathway assures the synthesis of HIF-1alpha protein in a glucose- and reoxygenation-dependent manner in irradiated tumors. *The Journal of biological chemistry* 2009;**284**: 5332-42.

25. Lu H, Liang K, Lu Y, Fan Z. The anti-EGFR antibody cetuximab sensitizes human head and neck squamous cell carcinoma cells to radiation in part through inhibiting radiation-induced upregulation of HIF-1alpha. *Cancer letters* 2012;**322**: 78-85.

26. Kim WY, Oh SH, Woo JK, Hong WK, Lee HY. Targeting heat shock protein 90 overrides the resistance of lung cancer cells by blocking radiation-induced stabilization of hypoxia-inducible factor-1alpha. *Cancer research* 2009;**69**: 1624-32.

27. Ichimura H, Yamasaki M, Tamura I, Katsumoto T, Sawada M, Kurimura O, Furuyama J, Kurimura T. Establishment and characterization of a new cell line TC-YIK originating from argyrophil small cell carcinoma of the uterine cervix integrating HPV16 DNA. *Cancer* 1991;**67**: 2327-32.

28. Saga Y, Suzuki M, Tamura N, Ohwada M, Sato I. Establishment and characterization of a new cell line (SKS) from neuroendocrine small cell carcinoma of the uterine cervix and its chemosensitivity. *Oncology* 2001;**60**: 367-72.

29. Siolas D, Hannon GJ. Patient-derived tumor xenografts: transforming clinical samples into mouse models. *Cancer research* 2013;**73**: 5315-9.

30. Begg AC. Predicting response to radiotherapy: evolutions and revolutions. *International journal of radiation biology* 2009;**85**: 825-36.

31. Begg AC. Predicting recurrence after radiotherapy in head and neck cancer. *Seminars in*

radiation oncology 2012;**22**: 108-18.

32. Dewhirst MW, Chi JT. Understanding the tumor microenvironment and radioresistance by combining functional imaging with global gene expression. *Seminars in radiation oncology* 2013;**23**: 296-305.

33. Ramsay J, Ward R, Bleehen NM. Radiosensitivity testing of human malignant gliomas. *International journal of radiation oncology, biology, physics* 1992;**24**: 675-80.

34. Girinsky T, Bernheim A, Lubin R, Tavakoli-Razavi T, Baker F, Janot F, Wibault P, Cosset JM, Duvillard P, Duverger A, et al. In vitro parameters and treatment outcome in head and neck cancers treated with surgery and/or radiation: cell characterization and correlations with local control and overall survival. *International journal of radiation oncology, biology, physics* 1994;**30**: 789-94.

35. Harma V, Virtanen J, Makela R, Happonen A, Mpindi JP, Knuuttila M, Kohonen P, Lotjonen J, Kallioniemi O, Nees M. A comprehensive panel of three-dimensional models for studies of prostate cancer growth, invasion and drug responses. *PloS one* 2010;**5**: e10431.

36. Debnath J, Brugge JS. Modelling glandular epithelial cancers in three-dimensional cultures. *Nature reviews Cancer* 2005;**5**: 675-88.

37. Semenza GL. Targeting HIF-1 for cancer therapy. *Nature reviews Cancer* 2003;**3**: 721-32.

38. Burri P, Djonov V, Aebersold DM, Lindel K, Studer U, Altermatt HJ, Mazzucchelli L, Greiner RH, Gruber Gü. Significant correlation of hypoxia-inducible factor-1α with treatment outcome in cervical cancer treated with radical radiotherapy. *International Journal of Radiation Oncology*Biology*Physics* 2003;**56**: 494-501.

39. Iyer NV, Kotch LE, Agani F, Leung SW, Laughner E, Wenger RH, Gassmann M, Gearhart JD, Lawler AM, Yu AY, Semenza GL. Cellular and developmental control of O2 homeostasis by hypoxia-inducible factor 1alpha. *Genes & Development* 1998;**12**: 149-62.

40. Ryan HE, Lo J, Johnson RS. HIF-1 alpha is required for solid tumor formation and embryonic vascularization. *The EMBO journal* 1998;**17**: 3005-15.

41. Gorski DH, Beckett MA, Jaskowiak NT, Calvin DP, Mauceri HJ, Salloum RM, Seetharam S, Koons A, Hari DM, Kufe DW, Weichselbaum RR. Blockage of the vascular endothelial growth factor stress response increases the antitumor effects of ionizing radiation. *Cancer research* 1999;**59**: 3374-8.

42. Akakura N, Kobayashi M, Horiuchi I, Suzuki A, Wang J, Chen J, Niizeki H, Kawamura K, Hosokawa M, Asaka M. Constitutive expression of hypoxia-inducible factor-1alpha renders pancreatic cancer cells resistant to apoptosis induced by hypoxia and nutrient deprivation. *Cancer research* 2001;**61**: 6548-54.

43. Unruh A, Ressel A, Mohamed HG, Johnson RS, Nadrowitz R, Richter E, Katschinski DM, Wenger RH. The hypoxia-inducible factor-1 alpha is a negative factor for tumor therapy. *Oncogene* 2003;**22**: 3213-20.

44. Moeller BJ, Dreher MR, Rabbani ZN, Schroeder T, Cao Y, Li CY, Dewhirst MW. Pleiotropic effects of HIF-1 blockade on tumor radiosensitivity. *Cancer cell* 2005;**8**: 99-110.

45. Liu YV, Baek JH, Zhang H, Diez R, Cole RN, Semenza GL. RACK1 competes with HSP90 for

binding to HIF-1alpha and is required for O(2)-independent and HSP90 inhibitor-induced degradation of HIF-1alpha. *Molecular cell* 2007;**25**: 207-17.

46. Bisht KS, Bradbury CM, Mattson D, Kaushal A, Sowers A, Markovina S, Ortiz KL, Sieck LK, Isaacs JS, Brechbiel MW, Mitchell JB, Neckers LM, et al. Geldanamycin and 17-allylamino-17-demethoxygeldanamycin potentiate the in vitro and in vivo radiation response of cervical tumor cells via the heat shock protein 90-mediated intracellular signaling and cytotoxicity. *Cancer research* 2003;**63**: 8984-95.

47. Bull EE, Dote H, Brady KJ, Burgan WE, Carter DJ, Cerra MA, Oswald KA, Hollingshead MG, Camphausen K, Tofilon PJ. Enhanced tumor cell radiosensitivity and abrogation of G2 and S phase arrest by the Hsp90 inhibitor 17-(dimethylaminoethylamino)-17-demethoxygeldanamycin. *Clinical cancer research : an official journal of the American Association for Cancer Research* 2004;**10**: 8077-84.

48. Camphausen K, Tofilon PJ. Inhibition of Hsp90: a multitarget approach to radiosensitization. *Clinical cancer research : an official journal of the American Association for Cancer Research* 2007;**13**: 4326-30.

Figure legends

Figure 1.

Characteristics of CTOSs from human SCCCs. (*a*) Phase-contrast images of a flow-through fraction, an organoids fraction, and CTOSs from a cerv-46 patient tumor. Scale bar indicates 200 μm. (*b*) Hematoxilin & eosin staining of original tumors, CTOS-derived xenografts, and CTOSs. Scale bars indicate 50 μm. (*c*) Immunohistochemistry of original tumors, CTOS-derived xenografts, and CTOSs using antibodies against neuroendocrine markers: chromogranin A, CD56, and synaptophysin. Scale bars indicate 50 μm.

Figure 2.

Radiation sensitivity assay using SCCC CTOSs. (*a*) CTOSs were irradiated at a dose of 0 or 7.5 Gy.

Representative images of each CTOS before and seven days after irradiation are shown. The cells that lost cell membrane integrity were visualized by propidium iodide staining (red) at day 7 after irradiation. Phase-contrast images of cerv-5 and cerv-9 CTOSs 7 days after 7.5 Gy irradiation are shown in higher magnification (bottom). Dotted lines indicate the edge of the core region of a viable CTOS. Scale bars indicate 100 μm. (*b* and *c*) Growth inhibition by radiation at indicated doses in all six SCCC CTOSs. The relative area (day 7/day 0) of the CTOSs adjusted to the non-irradiated CTOSs in each case is shown in (*b*); non-adjusted relative area (day 7/day 0) shown in (*c*). Data are given as means with S.D. ($n = 5$ per condition).

Figure 3.

Validation of CTOS radiation sensitivity assay. (*a*) Growth delay assay of xenograft tumors derived from cerv-5 , cerv21 and cerv-9. Mice were irradiated with 5 Gy at day 0. Data are given as means with S.D. ($n = 6$ tumors in 3 mice per group) $*p < 0.05$. (*b*) Gamma-H2AX foci formation assay with radio-resistant (cerv-5 and cerv21) and radio-sensitive (cerv-9 and cerv-46) CTOSs. Representative images of immunohistochemistry of irradiated or non-irradiated CTOSs using γ-H2AX antibody (red). Counterstaining was conducted with DAPI (blue). (*c*) Percentage of nuclei that were positive for γ-H2AX is shown. Data are means with S.D. ($n = 8–10$ per condition). (*d*) Western blot analysis of caspase-3 (Casp3) in CTOSs at indicated times after 5 Gy irradiation. Size of the bands is indicated.

Figure 4.

HIF-1α activity in CTOSs. (*a*) Gene set enrichment analysis plot of HIF-1α target genes in radio-resistant (cerv-5) versus radio-sensitive (cerv-9) CTOSs. The normalized enrichment score (NES) was 2.10, and the *p* value was <0.05. (*b*) RT-PCR for HIF-1α target genes in CTOSs. *GLUT1*, glucose transporter 1; *HK2*, hexokinase 2; *PDK1*, pyruvate dehydrogenase kinase, isozyme 1; *CA9*, carbonic anhydrase IX; *VEGF*, vascular endothelial growth factor. (*c*) Western blot analysis of HIF-1α expression in CTOSs at indicated times after 5 Gy irradiation. (*d*) Whole mount immunostaining of cerv-5 CTOSs before and 4 hours after 5 Gy irradiation using HIF-1α antibody (red). Counterstaining was conducted with Hoechst33342 (blue). CTOS cultured in hypoxia (1% O_2) was used as a positive control.

Figure. 5

The mechanism of increased HIF-1α protein levels in cerv-5 CTOSs. (*a*) Representative images of pimonidazole staining of non-irradiated or irradiated (4 hours after 5 Gy irradiation) CTOSs. CTOS cultured in hypoxia (1% O_2) was used as a positive control. *IR*, irradiation. (*b*) Representative images of non-irradiated or irradiated CTOSs labeled with ROS-sensitive dye, DCFDA. CTOSs treated with N-acetylcysteine (NAC), a ROS scavenger, were used as a negative control. DMSO was used as a vehicle control. Scale bars indicate 100 μm. (*c*) Western blot analysis of HIF-1α expression and pS6

in irradiated CTOSs. CTOSs were irradiated at a dose of 5 Gy immediately after addition of indicated doses of RAD001 and lysed 4 hours after irradiation. (*d*) Western blot analysis of radiation-induced HIF-1α expression in CTOSs treated with 17-AAG. CTOSs were irradiated at a dose of 5 Gy immediately after addition of the indicated doses of 17-AAG and lysed 4 hours after irradiation.

Figure 6.

Role of HIF-1α in radiation resistance in cerv-5. (*a*) The efficacy of HIF-1α knockdown in cerv-5 CTOSs. Representative images of whole mount immunostaining of CTOSs cultured in hypoxia (1% O_2) using HIF-1α antibody (red). (*b*) Radiation sensitivity in combination with HIF-1α inhibition by shRNA/HIF-1α (left and middle) or 17-AAG (1 μM) (right). The relative area (day 7/day 0) of the CTOSs adjusted to the control CTOSs is shown. Data given as means with S.D. ($n = 5$ per condition). *$p < 0.05$, **$p < 0.001$, and ***$p < 0.0001$. (*c*) Western blot analysis of caspase-3 (Casp3) and cleaved caspase-3 (Cl-casp3) in control and HIF-1α-knockdown CTOSs at indicated time after 5 Gy irradiation.

Supplementary materials and methods

Quantitative RT-PCR

Total RNA was isolated by the RNeasy Mini kit (Qiagen) from CTOSs, and by NucleoSpin totalRNA FFPE (Macherey-Nagel, Duren, Germany) from original tumor samples. One microgram of total RNA was reverse transcribed to obtain cDNA using Superscript III (Invitrogen) according to the manufacturer's protocol. The quantitative PCR reactions were performed with the StepOne Real Time PCR System (Life Technologies, Carlsbad, CA) using Fast SYBR Green Master MIX. The Comparative C_T Method ($\Delta\Delta C_T$ Method) was applied according to the manufacture's instruction. Fold difference to the control sample (cerv-51, adenocarcinoma of the cervix) is shown. The primer sequences are given in Supplementary Table 1.

Supplementary figure legends

Figure S1.

Quantitative RT-PCR for neuroendocrime markers in original patient tumors (upper panels) and CTOSs (lower panels). *CHGA*, chromogranin A; *NCAM1*, neural cell adhesion molecule 1; *SYP*, synaptophysin.

Figure S2.

Radiosensitivity assay using patients-derived CTOSs. The relative area (day 7/day 0) of the CTOSs adjusted to the non-irradiated CTOSs in each case is shown in (*a*); non-adjusted relative area (day 7/day 0) shown in (*b*). Data are given as means with S.D. (n = 3-5 per condition).

Figure S3.

(*a*) Quantitative RT-PCR for HIF-1α and its target genes. HIF1A, hypoxia-inducible factor-1α; *VEGFA*, vascular endothelial growth factor A; *SLC2A1*, solute carrier family 2 (facilitated glucose transporter), member 1. (*b*) Western blot analysis of HIF-2α expression at basal levels in CTOSs. Cerv-5 CTOS cultured in hypoxia (1% O_2) was used as a positive control.

Figure S4.

(*a*) RT-PCR for HIF-1α target genes in HIF-1α knockdown cerv-5 CTOSs. (*b*) Dose-response curve of 17-AAG in

cerv-5 CTOS. Each CTOS was embedded in a gel droplet of Matrigel GFR and cultured in StemPro hESC containing 17-AAG at indicated doses. CTOSs were exposed to 17-AAG for an initial 72 hours, then washed and incubated without drug afterwards. The relative area (day 7/day 0) of the CTOSs adjusted to the non-treated CTOSs is shown. Data given as means with S.D. (n = 5 per condition). The sigmoidal dose-response curve was drawn with GraphPad Prism6.

Figure S5.

(*a*) Dose-response curve of 17-AAG in all five CTOSs. (*b*) The effect of 17-AAG (1 μM) alone, radiation (2.5 Gy) alone, or combination of both in 5 CTOSs. The relative area (day 7/day 0) of the CTOSs adjusted to the control CTOSs is shown. Data given as means with S.D. (n = 5 per condition).

figure 1

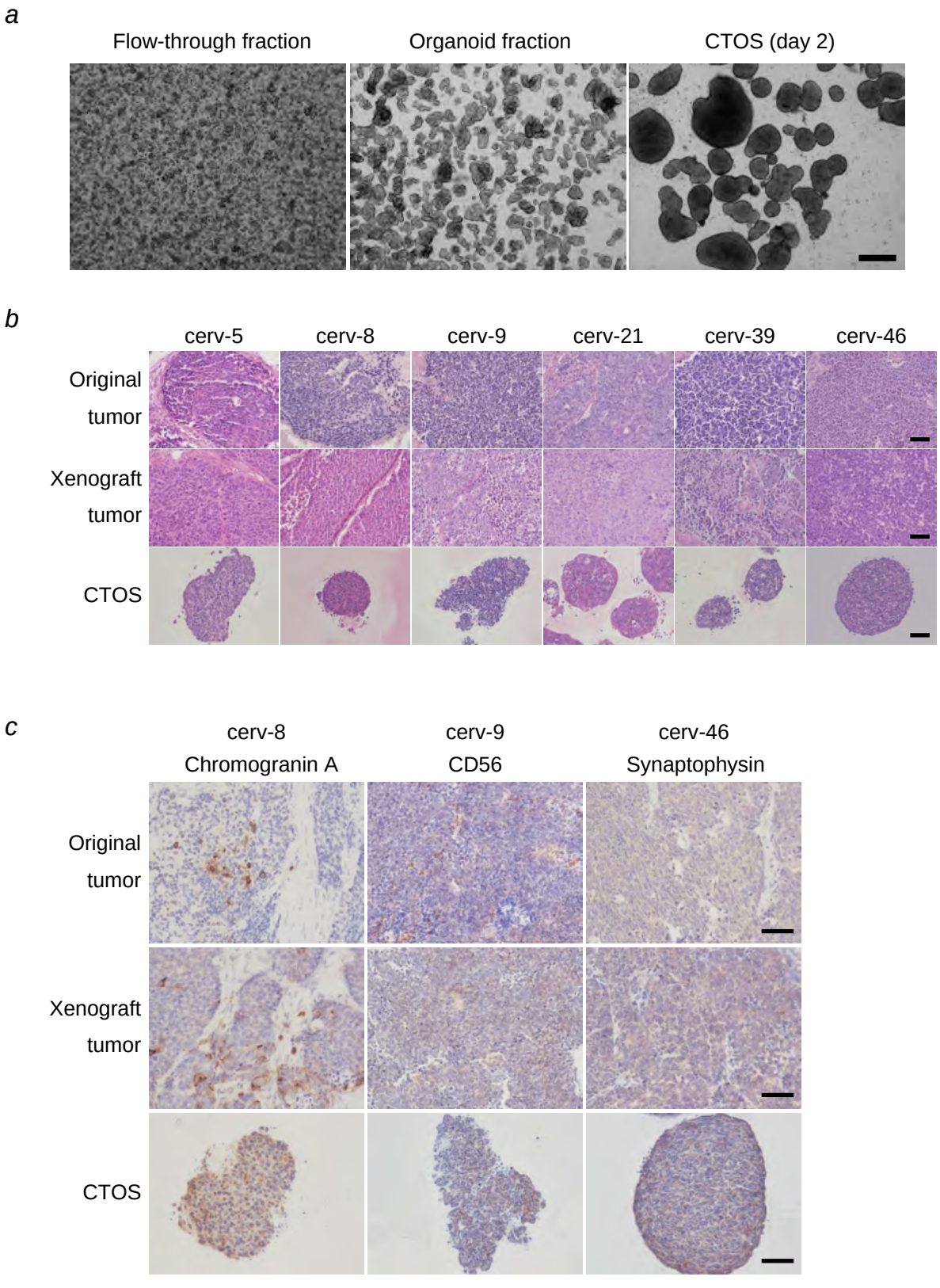
a
Flow-through fraction
Organoid fraction
CTOS (day 2)
b
cerv-5
cerv-8
cerv-9
cerv-21
cerv-39
cerv-46
Original tumor
Xenograft tumor
CTOS
c
cerv-8
Chromogranin A
cerv-9
CD56
cerv-46
Synaptophysin
Original tumor
Xenograft tumor
CTOS

figure 2

a

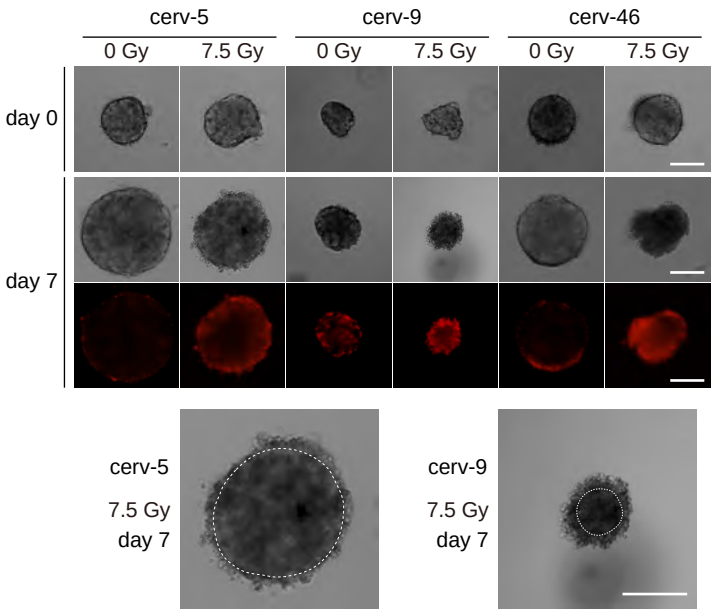
cerv-5
cerv-9
cerv-46
0 Gy
7.5 Gy
0 Gy
7.5 Gy
0 Gy
7.5 Gy
day 0
day 7
cerv-5
7.5 Gy
day 7
cerv-9
7.5 Gy
day 7

b

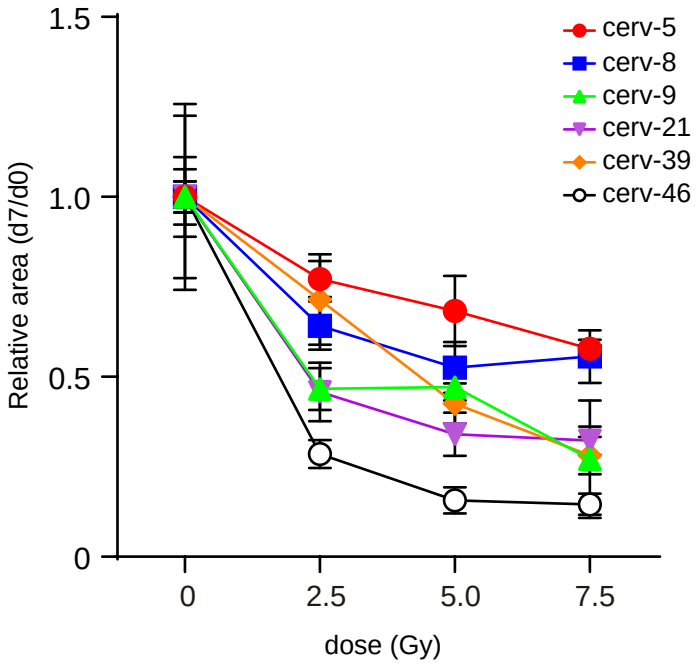
1.5
1.0
0.5
0
Relative area (d7/d0)
0
2.5
5.0
7.5
dose (Gy)
cerv-5
cerv-8
cerv-9
cerv-21
cerv-39
cerv-46

c

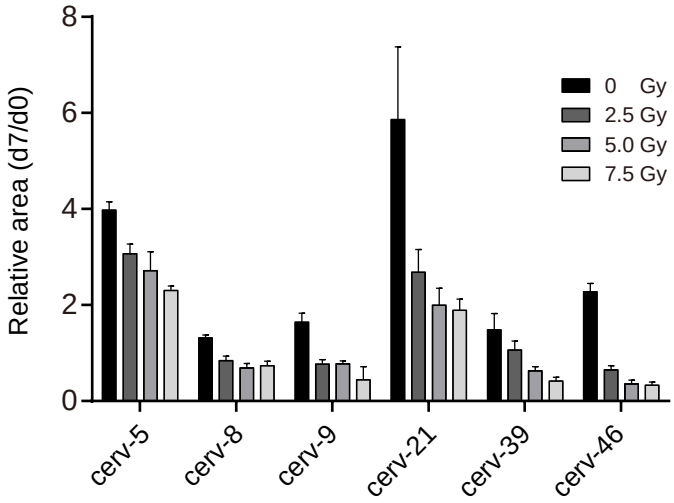
8
6
4
2
0
Relative area (d7/d0)
0 Gy
2.5 Gy
5.0 Gy
7.5 Gy
cerv-5
cerv-8
cerv-9
cerv-21
cerv-39
cerv-46

figure 3

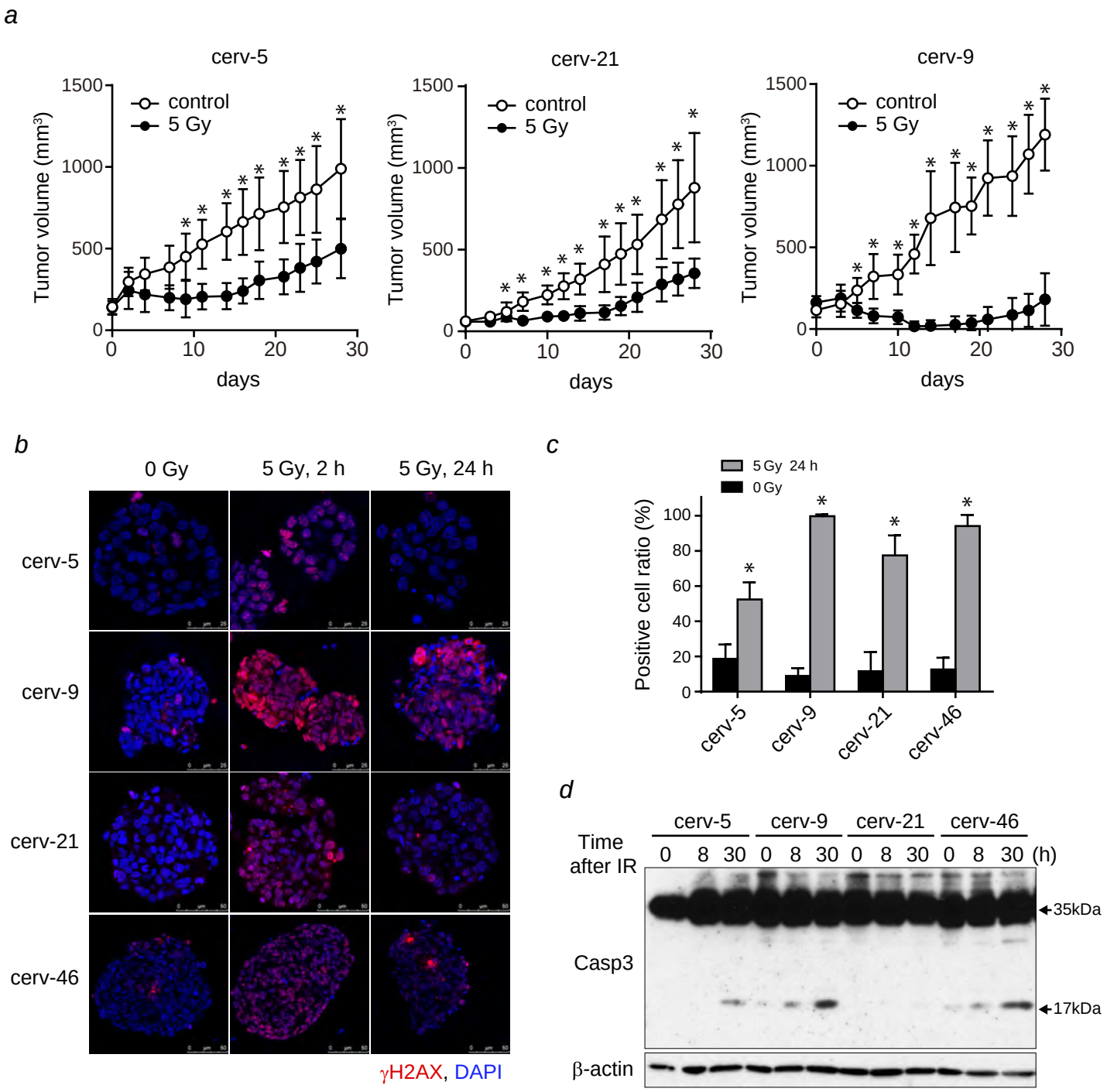
a
cerv-5
cerv-21
cerv-9
control
5 Gy
Tumor volume (mm³)
days
b
0 Gy
5 Gy, 2 h
5 Gy, 24 h
cerv-5
cerv-9
cerv-21
cerv-46
γH2AX, DAPI
c
5 Gy 24 h
0 Gy
Positive cell ratio (%)
cerv-5
cerv-9
cerv-21
cerv-46
d
cerv-5
cerv-9
cerv-21
cerv-46
Time after IR
0 8 30 0 8 30 0 8 30 0 8 30 (h)
35kDa
17kDa
Casp3
β-actin

figure 4

a

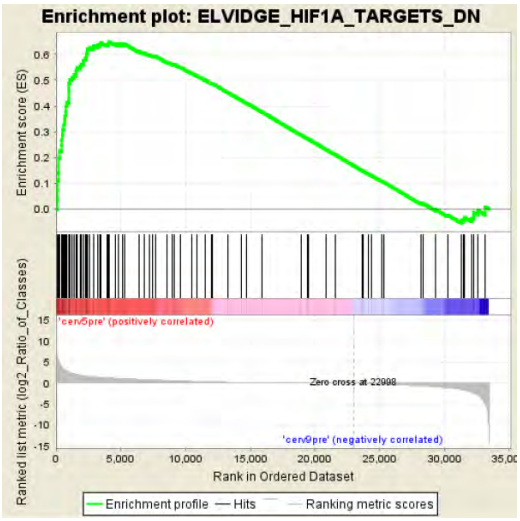

b

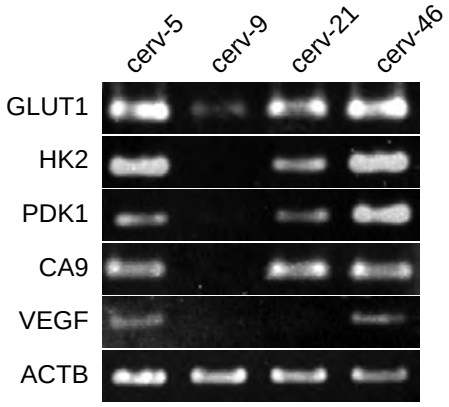

c

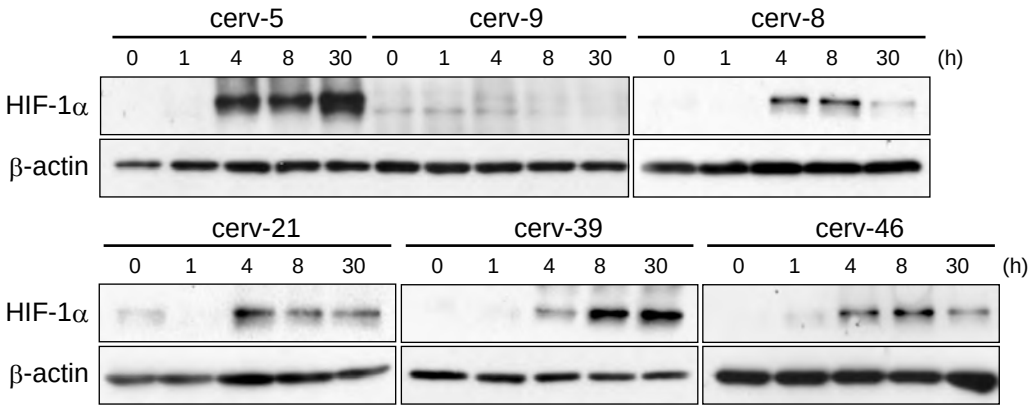

d

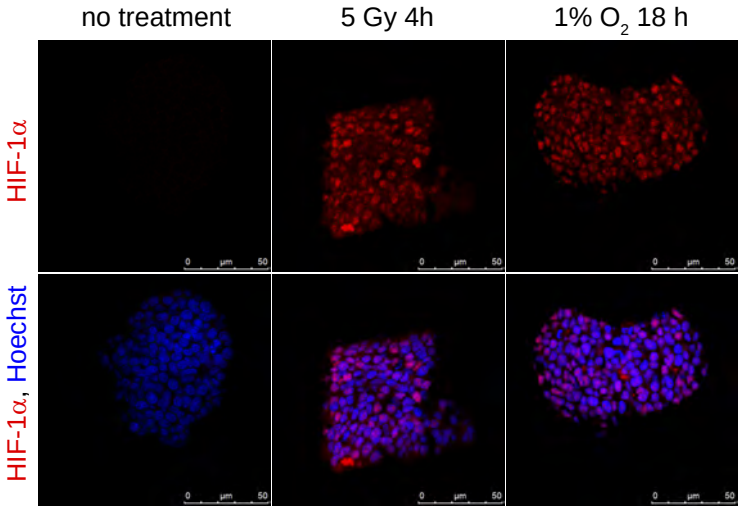

figure 5

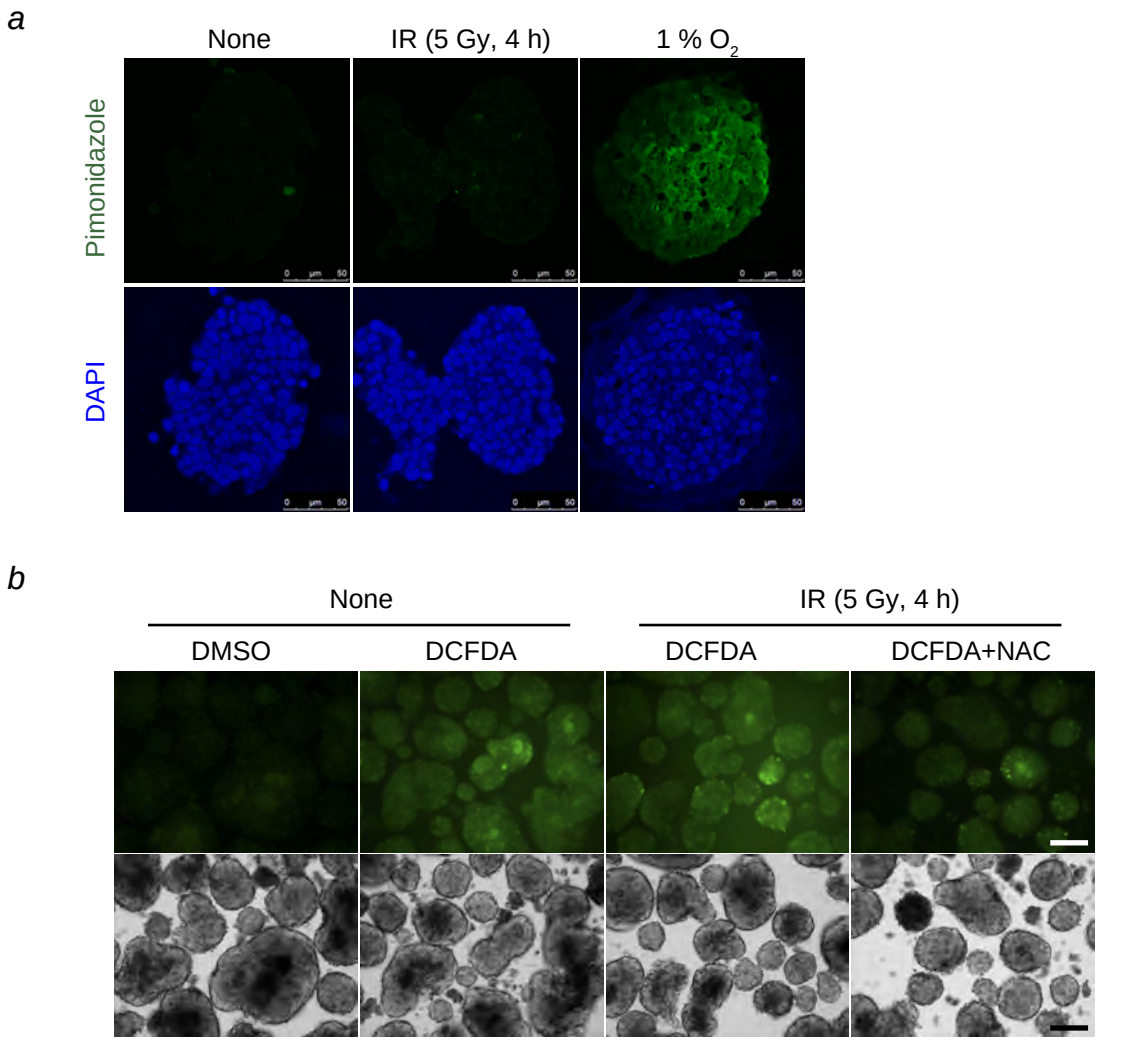
a
None
IR (5 Gy, 4 h)
1 % O2
Pimonidazole
DAPI
b
None
IR (5 Gy, 4 h)
DMSO
DCFDA
DCFDA
DCFDA+NAC
c
IR
None
5 Gy
RAD001
0
0
0.001
0.01
0.1
1
(μM)
HIF-1α
pS6
β-actin
d
IR
None
5 Gy
17-AAG
0
0
0.1
1
(μM)
HIF-1α
β-actin

figure 6

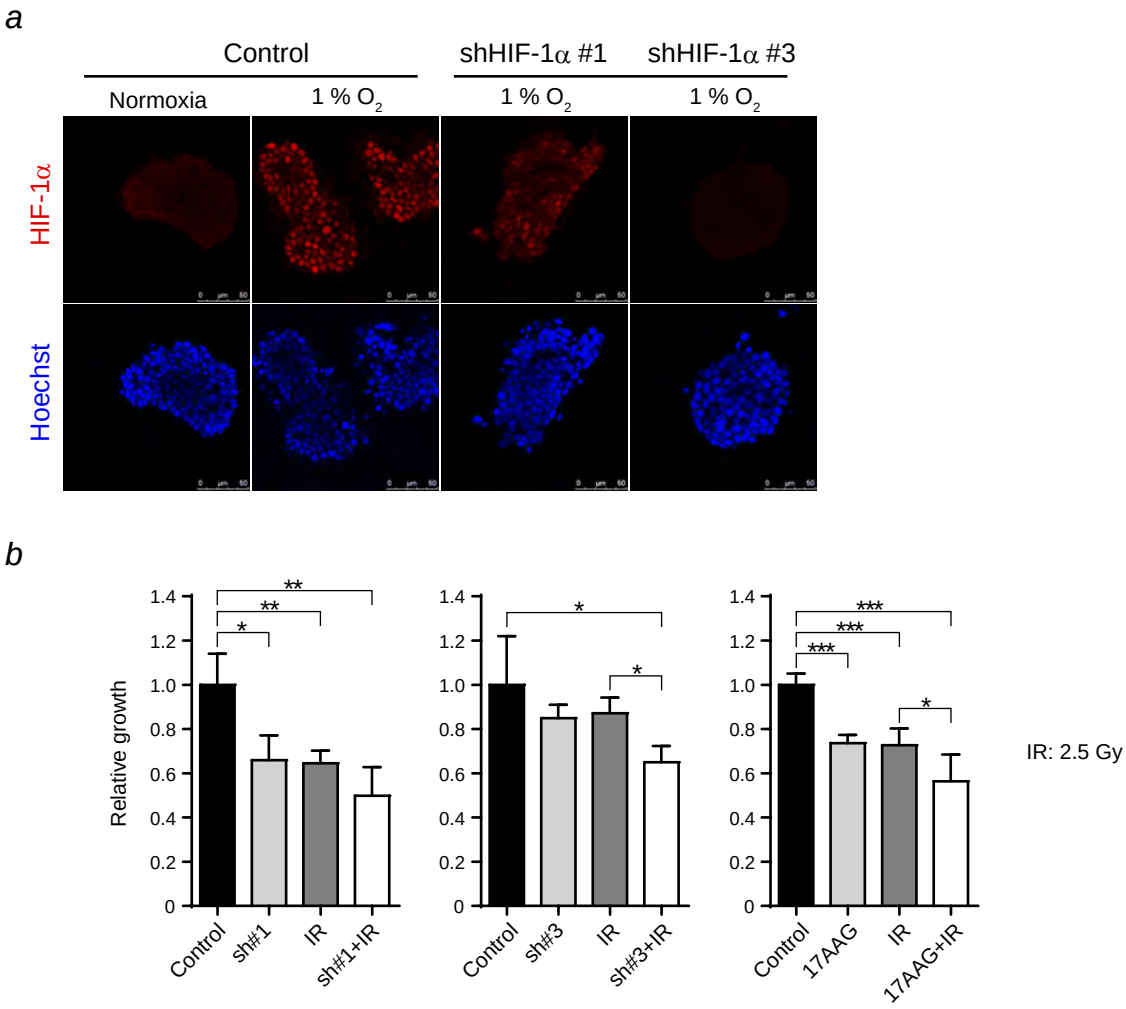
a
Control
shHIF-1α #1
shHIF-1α #3
Normoxia
1 % O2
1 % O2
1 % O2
HIF-1α
Hoechst
b
Relative growth
Control
sh#1
IR
sh#1+IR
Control
sh#3
IR
sh#3+IR
Control
17AAG
IR
17AAG+IR
IR: 2.5 Gy
c
Control
shHIF-1α #3
Time after IR
0 8 30 0 8 30 (h)
HIF-1α
Casp3
35 kDa
17 kDa
Cl-casp3
19 kDa
17 kDa
β-actin

Supplementary Table 1

Primer sequences used in RT-PCR

Gene	Forward	Reverse
GLUT1	cttcactgtcgtgtcgctgt	tgaagagttcagccacgatg
HK2	ccacctttgtgaggtccact	gtcctcagggatggcataga
PDK1	gaagcagttcctggacttcg	accaattgaacggatggtgt
CA9	acttcagccgctacttccaa	tcagctgtagccgagagtca
VEGFA	aaggaggagggcagaatcat	atctgcatggtgatgttgga
*HIF1A**	tggacttgcctttccttctc	gaagtggcaactgatgagca
ACTB	ggacttcgagcaagagatgg	agcactgtgttggcgtacag
CHGA	cctgtcagccaggaatgttt	ggggtactcgaactcgacct
NCAM1	aatgtgccacctaccatcca	agatgtactcagcctcgtcg
SYP	acatggacgtggtgaatcag	ggggtactcgaactcgacct
HIF1A‡	cagtcgacacagcctggata	actgtcctgtggtgacttgt
SLC2A1	cttcactgtcgtgtcgctgt	tgaagagttcagccacgatg

* for semi-quantitative RT-PCR

‡ for quantitative RT-PCR

Supplementary Table 2

Sample ID	Patient age	Histology	Pathological stage			FIGO stage
			T	N	M	
cerv5	47	SCNEC	1b2	1	0	IB2
cerv8	44	LCNEC > SCNEC	2b2	1	0	IIB
cerv9	28	SCNEC	1b2	1	0	IB2
cerv21	22	SCNEC with endometrioid adenoca.	1b1	0	0	IB1
cerv39	37	SCNEC	1b2	0	0	IB2
cerv46	35	SCNEC	1b2	0	0	IB2

SCNEC= small cell neuroendocrine carcinoma

LCNEC= large cell neuroendocrine carcinoma

Figure S1

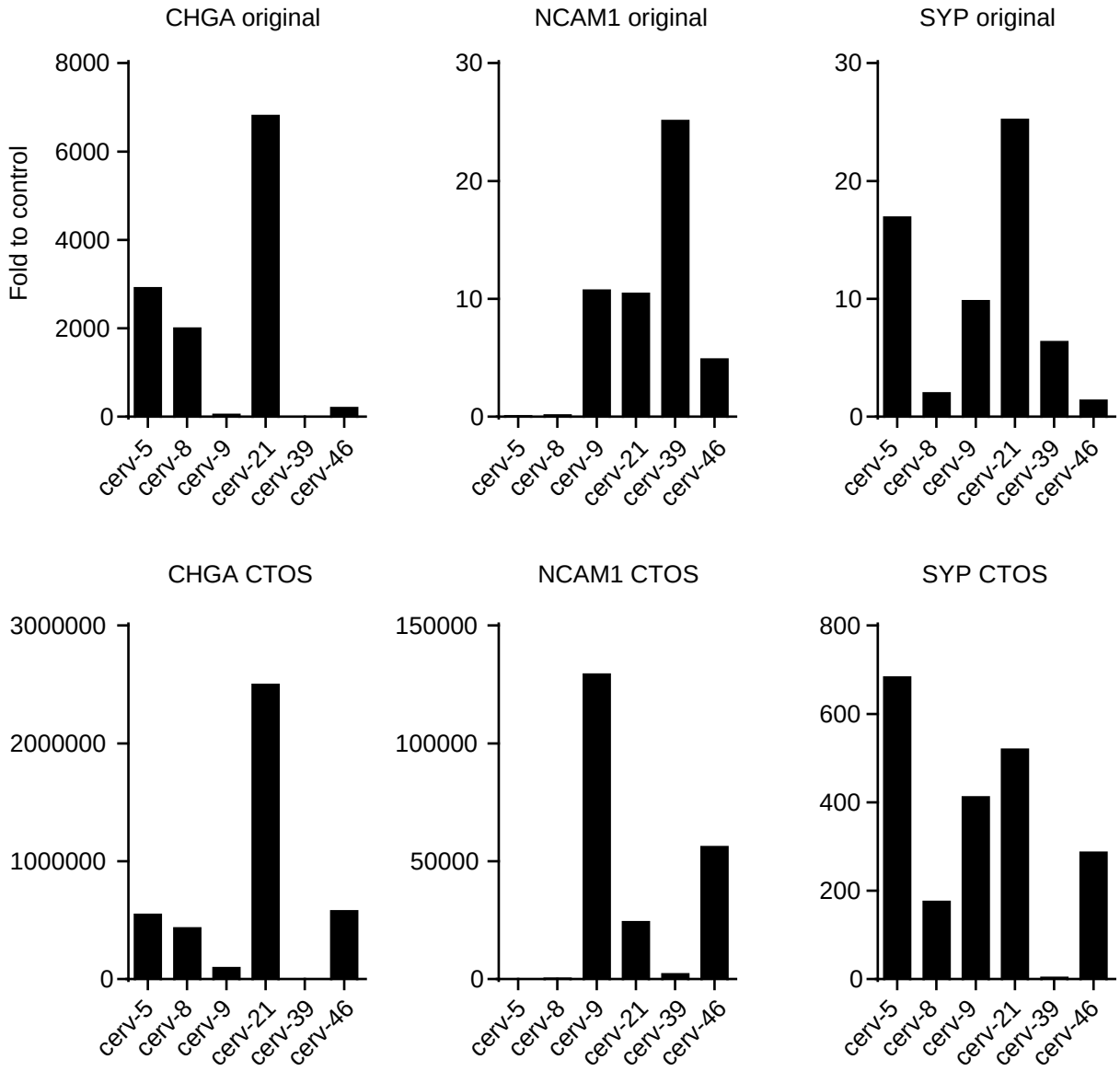
CHGA original
NCAM1 original
SYP original
Fold to control
8000
6000
4000
2000
0
30
20
10
0
30
20
10
0
cerv-5
cerv-8
cerv-9
cerv-21
cerv-39
cerv-46
CHGA CTOS
NCAM1 CTOS
SYP CTOS
3000000
2000000
1000000
0
150000
100000
50000
0
800
600
400
200
0

Figure S2

a

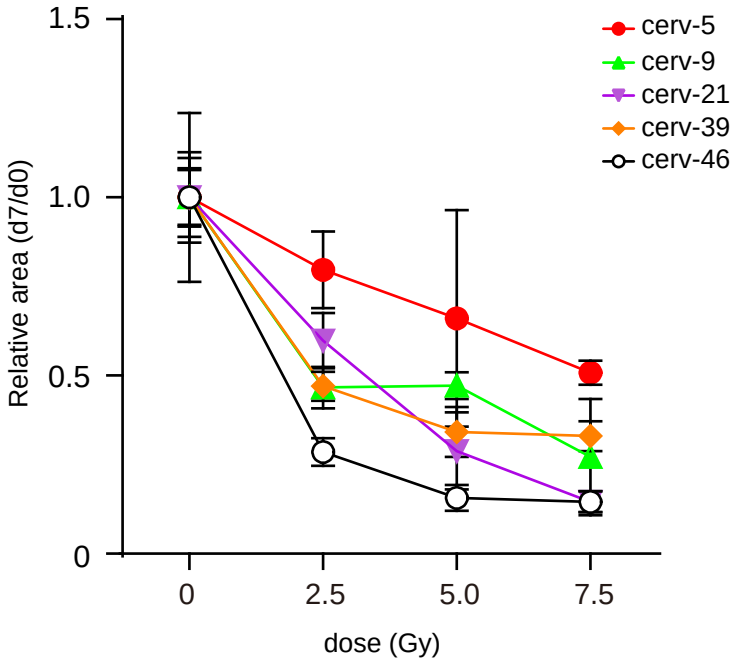
1.5
1.0
0.5
0
Relative area (d7/d0)
0
2.5
5.0
7.5
dose (Gy)
cerv-5
cerv-9
cerv-21
cerv-39
cerv-46

b

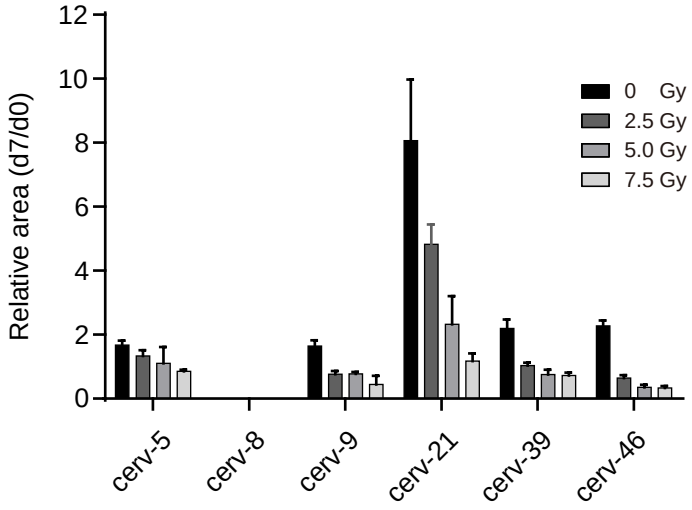
12
10
8
6
4
2
0
Relative area (d7/d0)
0 Gy
2.5 Gy
5.0 Gy
7.5 Gy
cerv-5
cerv-8
cerv-9
cerv-21
cerv-39
cerv-46

Figure S3

a

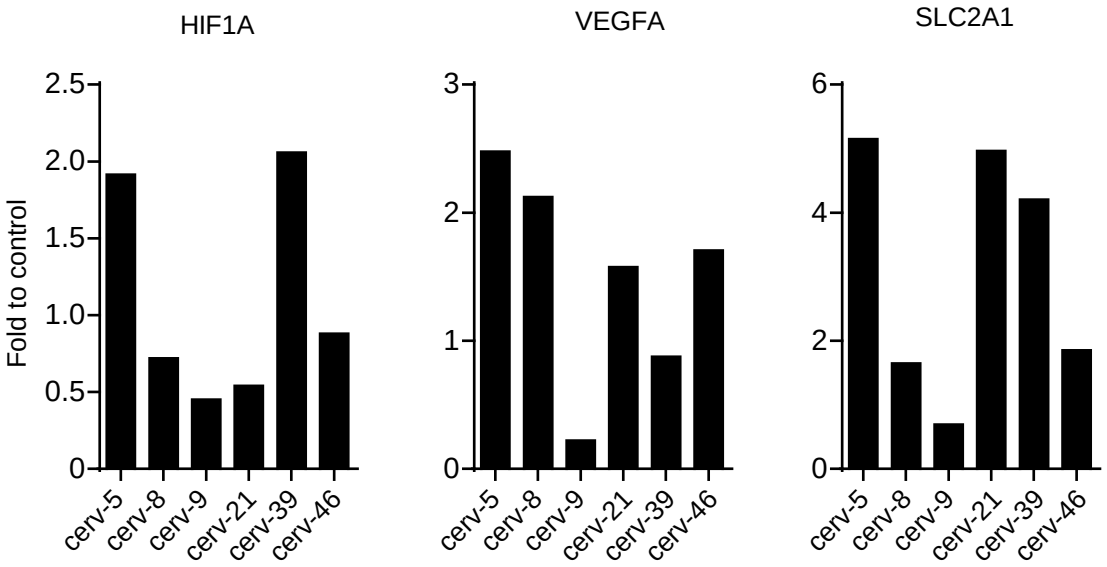
HIF1A
VEGFA
SLC2A1
Fold to control
2.5
2.0
1.5
1.0
0.5
0
3
2
1
0
6
4
2
0
cerv-5
cerv-8
cerv-9
cerv-21
cerv-39
cerv-46

b

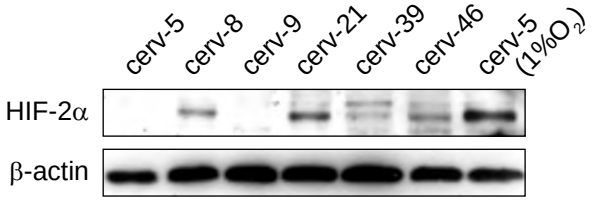
cerv-5
cerv-8
cerv-9
cerv-21
cerv-39
cerv-46
cerv-5 (1%O2)
HIF-2α
β-actin

Figure S4

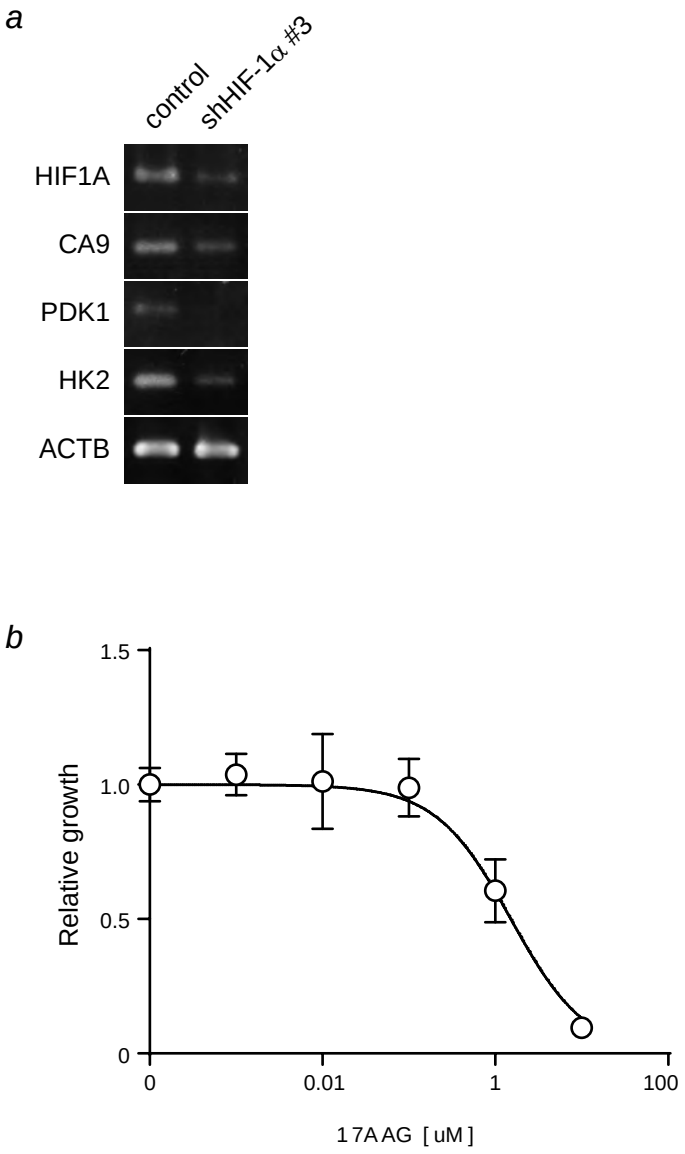
a
control
shHIF-1α #3
HIF1A
CA9
PDK1
HK2
ACTB
b
Relative growth
1.5
1.0
0.5
0
0
0.01
1
100
17AAG [uM]

Figure S5

a

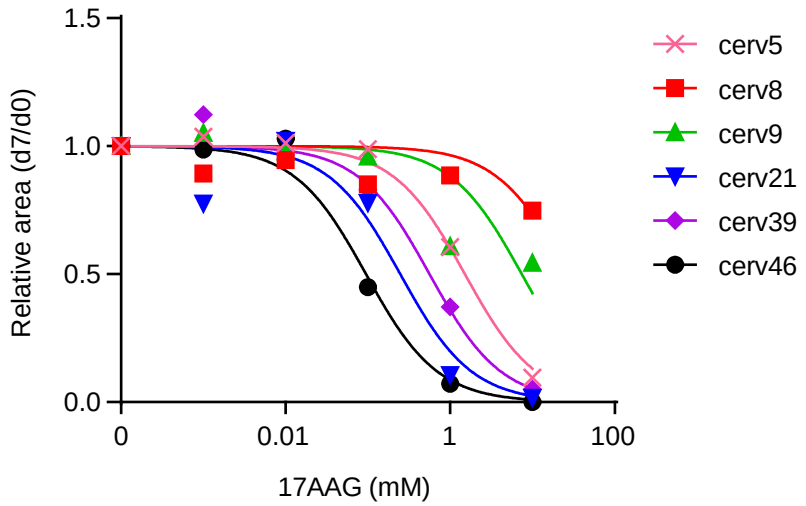
1.5
1.0
0.5
0.0
Relative area (d7/d0)
0
0.01
1
100
17AAG (mM)
cerv5
cerv8
cerv9
cerv21
cerv39
cerv46

b

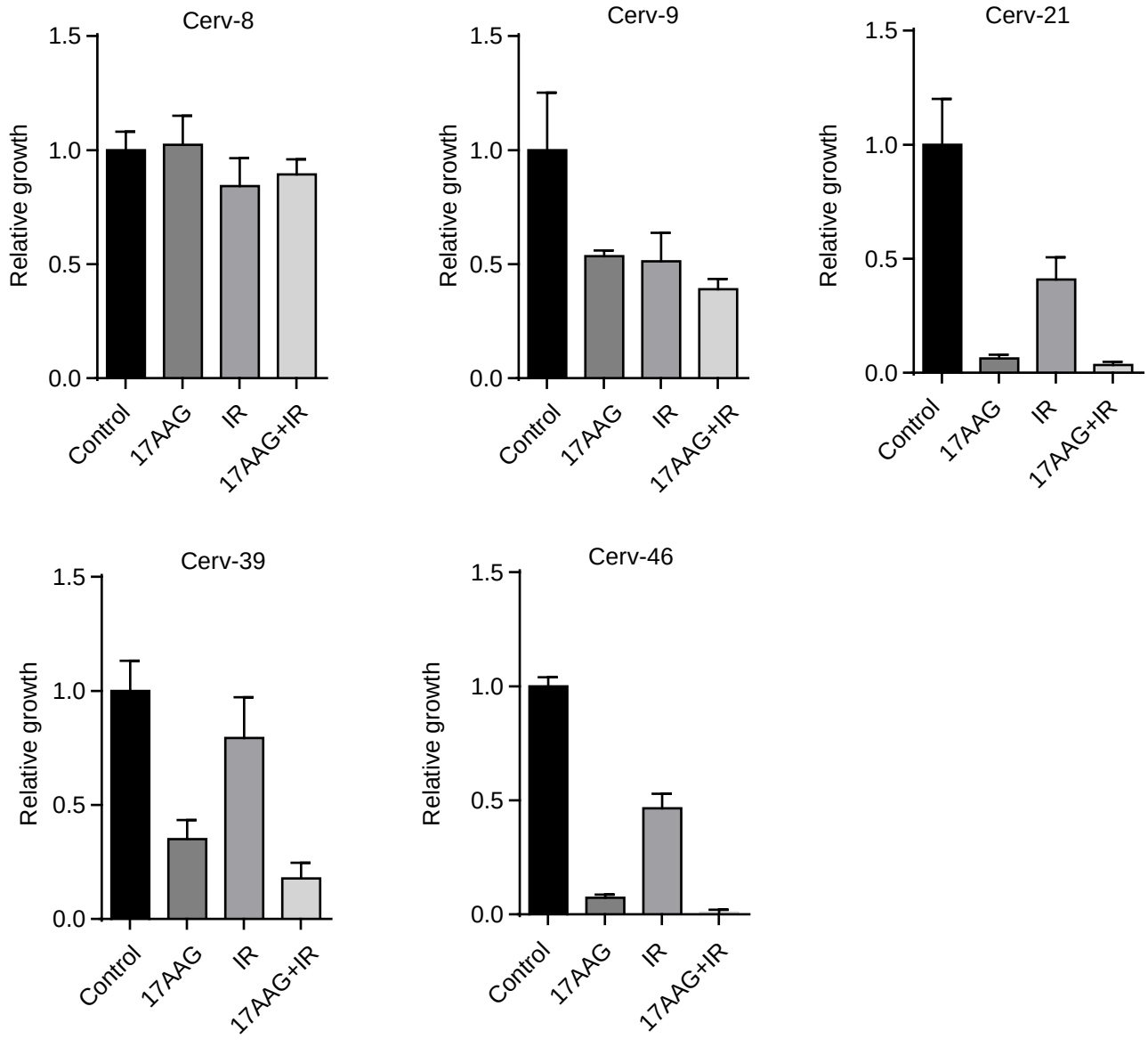
Cerv-8
Cerv-9
Cerv-21
Cerv-39
Cerv-46
Relative growth
1.5
1.0
0.5
0.0
Control
17AAG
IR
17AAG+IR